ANL-HEP-CP-80-07

CONF-791174--2

REVIEW OF NUCLEON-NUCLEON SCATTERING EXPERIMENTS
AND
MANY DINUCLEON RESONANCES

MASTER

by

Akihiko Yokosawa

Prepared for

1979 INS Symposium

on

Particle Physics in GeV Region

Tokyo, Japan

November 1979

ARGONNE NATIONAL LABORATORY, ARGONNE, ILLINOIS

U of C-AUA-USDOE

Operated under Contract W-31-109-Eng-38 for the

U. S. DEPARTMENT OF ENERGY

For the Proceedings of the
1979 INS Symposium on
Particle Physics in
GeV Region
Tokyo, Japan, November 1979
ANL-HEP-CP-80-07

REVIEW OF NUCLEON-NUCLEON SCATTERING EXPERIMENTS AND MANY DINUCLEON RESONANCES*

Akihiko Yokosawa
High Energy Physics Division
Argonne National Laboratory
9700 South Cass Avenue
Argonne, Illinois 60439

January 20, 1980

Abstract

We review structures appearing in various experimental data (particularly those with polarized beams) in nucleon-nucleon systems. We present a number of candidates for dibaryon resonances which can couple to nucleon-nucleon systems.

* Work supported by the U.S. Department of Energy.

Contents

I. Introduction

We would like to start out by discussing the proton-proton total cross-section data at the intermediate-energy region. As shown in Fig. 1, up to 1.2-GeV/c incident proton momentum, the total cross section, which mainly consists of the elastic process, falls and then rises due to the inelastic-channel opening. The cross section flattens above 1.5 GeV/c. We observe no structures that may suggest the possible existence of a resonance.

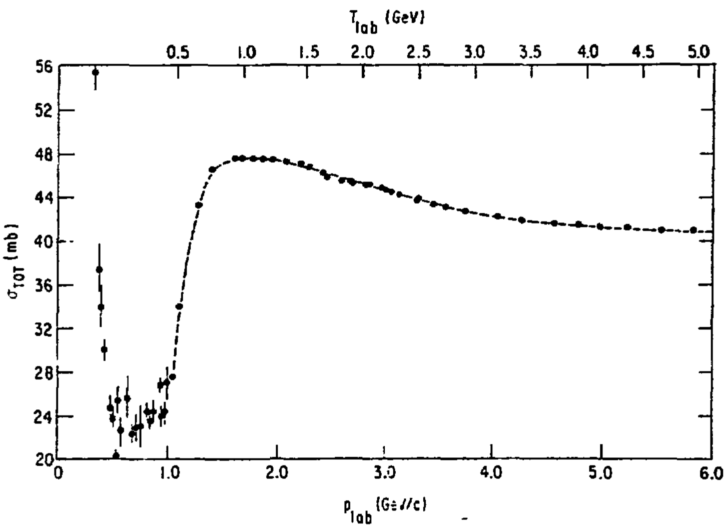

Fig. 1 pp Total Cross Section

However, we have observed totally unexpected structures in the total cross section when both the incident protons and target protons were longitudinally polarized. The most remarkable structure appears around $p_{lab} \approx 1.2$ and 1.5 GeV/c.

We discuss the existence of dibaryon resonances which can couple to dinucleon systems and their properties. Such a resonance opens a new era in the nucleon-nucleon system and also is crucially important for further development of the quark models that require six quarks in a bag.[1-4]

First, we describe experimental observables in terms of the helicity amplitudes, and then in terms of singlet and triplet partial-wave amplitudes. *There are three* s-channel helicity amplitudes at $\theta_{c.m.} = 0$:

$$\phi_1 = \langle ++|++\rangle,$$

$$\phi_2 = \langle --|++\rangle, \text{ and}$$

$$\phi_3 = \langle +-|+-\rangle \ .$$

These amplitudes are related to total cross section as follows:

i) Spin averaged total cross section

$$\sigma^{Tot} = (2\pi/k)\mathrm{Im}\{\phi_1(0) + \phi_3(0)\} = (1/2)\{\sigma^{Tot}(\rightleftarrows) + \sigma^{Tot}(\rightrightarrows)\} \qquad (1)$$

ii) Difference between total cross sections for parallel and antiparallel spin states (longitudinal)

$$\Delta\sigma_L = (4\pi/k)\mathrm{Im}\{\phi_1(0) - \phi_3(0)\} = \{\sigma^{Tot}(\rightleftarrows) - \sigma^{Tot}(\rightrightarrows)\} \qquad (2)$$

iii) Difference between total cross sections for parallel and antiparallel spin states (transverse)

$$\Delta\sigma_T = -(4\pi/k)\mathrm{Im}\ \phi_2(0) = \sigma^{Tot}(\uparrow\downarrow) - \sigma^{Tot}(\uparrow\uparrow) \qquad (3)$$

Argonne ZGS facilities provide various spin directions of incident beam and target. Spin directions are illustrated below.

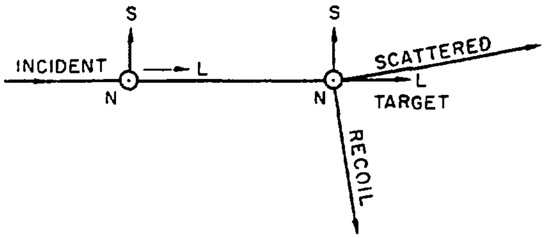

N: NORMAL TO THE SCATTERING PLANE
L: LONGITUDINAL DIRECTION
S = N x L IN THE SCATTERING PLANE

To express observables in elastic scattering, we adopt the notation (Beam, Target; Scattered, Recoil); (0,N;0,0) for polarization, (N,N;0,0) and (L,L;0,0) for spin correlation parameters, etc. A typical experimental setup for $\Delta\sigma_L$ is shown in Fig. 2 (a). The measurements were done in standard transmission experiment.

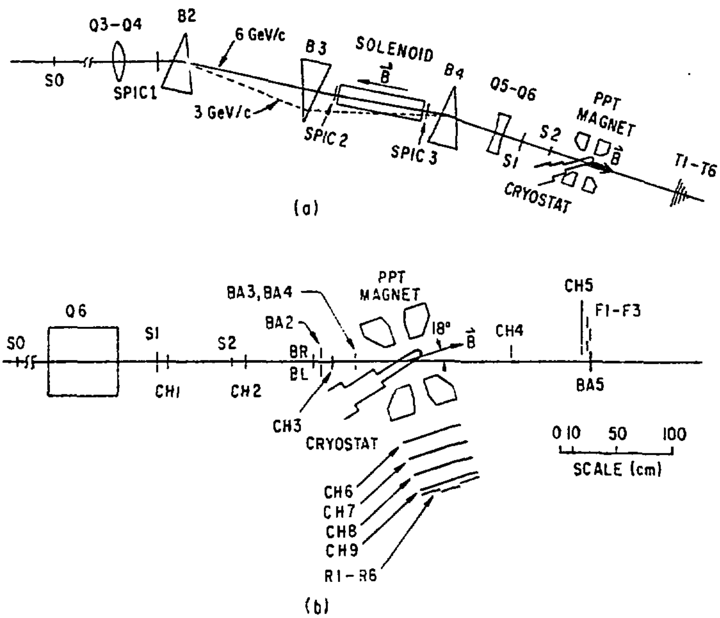

Fig. 2 (a) Beam line for the $\Delta\sigma_L$ measurement.
(b) Experimental setup for elastic-scattering measurements.

II. $\Delta\sigma_L(I=1)$ and $\Delta\sigma_T(I=1)$ Measurements

We show the results of $\Delta\sigma_L$ measurements from 1.0 to 6.0 GeV/c (Fig. 3a).[5-7] There is a sharp peak near 1.2 GeV/c and a dip near 1.5 GeV/c. From Eq. 2, a structure in $\phi_1(0)$ and $\phi_3(0)$ should appear as a peak and dip, respectively, in $\Delta\sigma_L$. Figure 3b shows $\sigma^{Tot}(\rightleftarrows)$ and $\sigma^{Tot}(\leftrightarrows)$ as obtained from Eqs. 1 and 2. There is a clear bump in $\sigma^{Tot}(\leftrightarrows)$. We observe the third structure in $\sigma^{Tot}(\rightleftarrows)$ near 2.0 GeV/c although that is not as remarkable as the one appearing in $\Delta\sigma_T$ which will be discussed later. Several momentum points between 3 and 6 GeV/c have recently been measured as shown in Fig. 3a.

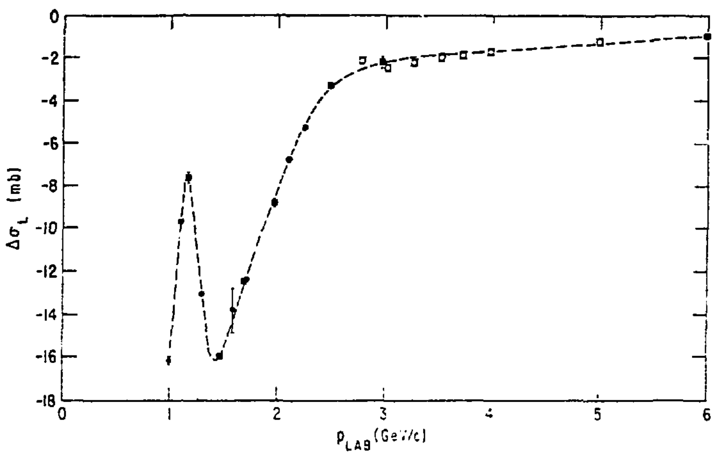

Fig. 3a Total cross-section difference $\Delta\sigma_L = \sigma^{Tot}(\leftrightarrows) - \sigma^{Tot}(\rightleftarrows)$. The white circles are preliminary data.

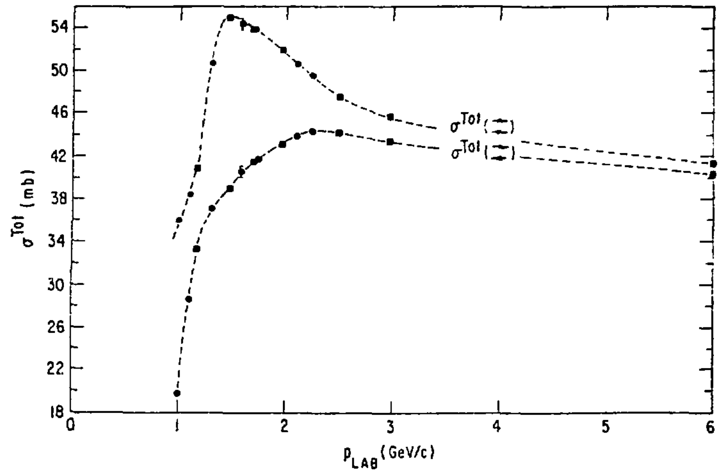

Fig. 3b Total cross sections for pure initial spin state. The dotted curves are only to guide the eye.

In Fig. 4, results of several $\Delta\sigma_L$ measurements up to 12 GeV/c are shown. Note that $\Delta\sigma_L \approx - 500$ μb at 12 GeV/c.

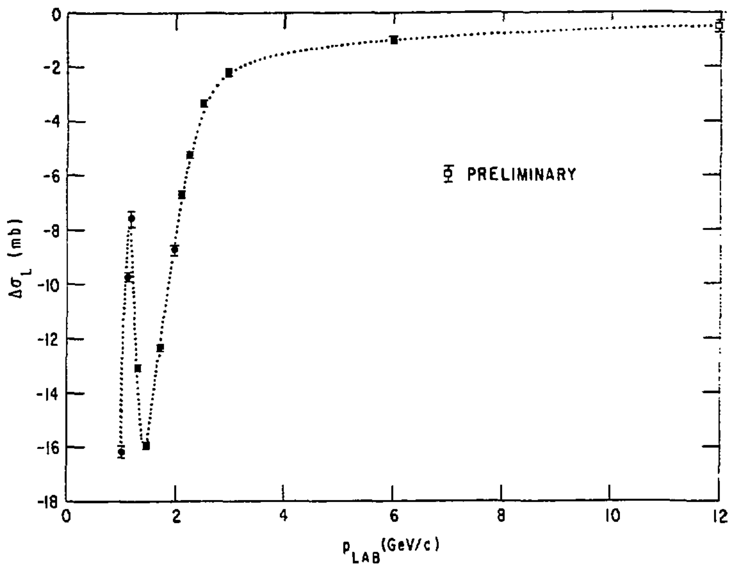

Fig. 4 Total cross section difference, $\Delta\sigma_L$, up to 12 GeV/c.

To study the behavior in terms of the partial scattering amplitudes, the data on $(k^2/4\pi)\Delta\sigma_T$ are plotted in Fig. 5 as a function of the center-of-mass energy,[8] where k is the c.m. momentum. If the dip in $\Delta\sigma_L$ is considered to be due to a resonance, the mass is about 2260 MeV with a width of about 200 MeV. The 1.2-GeV/c peak is seen in $\Delta\sigma_L$ and possibly in $\Delta\sigma_T$ data. The 2.0-GeV/c peak is clearly visible in $\Delta\sigma_T$.

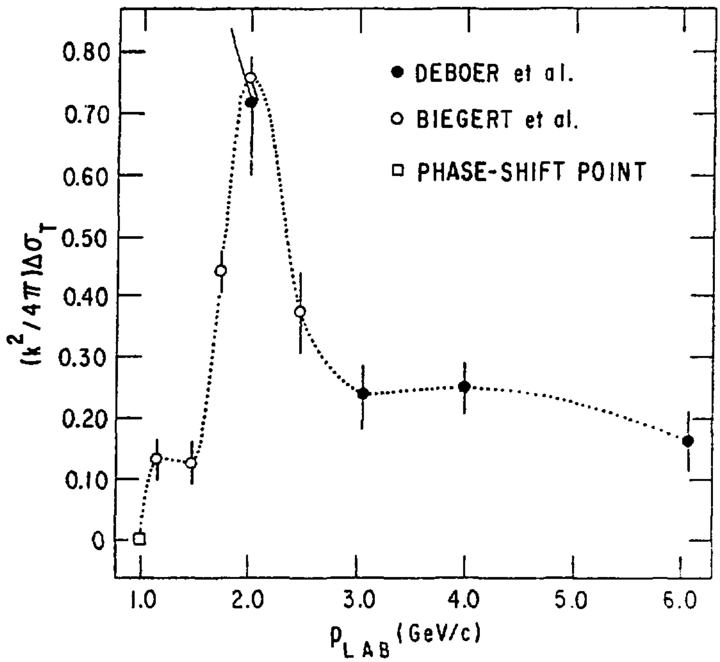

Fig. 5 Total cross-section difference $\Delta\sigma_T = \sigma^{Tot}(\uparrow\downarrow) - \sigma^{Tot}(\uparrow\uparrow)$

Using the data on $\Delta\sigma_L$, Grein and Kroll have calculated the real part of $[\phi_1(0) - \phi_3(0)]$ by applying dispersion relations.[9] In the Argand plot of the $[\phi_1(0) - \phi_3(0)]$ amplitude, we observe a clear resonance-like behavior around the incident proton momentum of 1.5 GeV/c (mass $\approx$ 2260 MeV) and possibly at 1.2 GeV/c (mass $\approx$ 2100 MeV) as shown in Fig. 6.

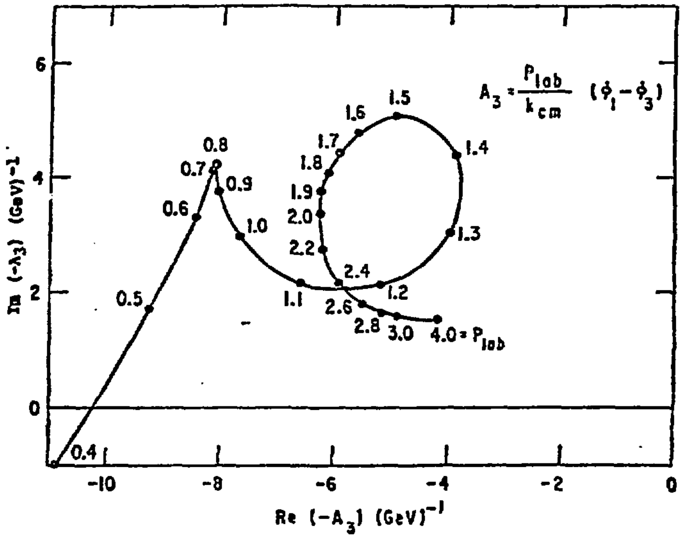

Fig. 6 Argand plot of the $[\phi_1(0) - \phi_3(0)]$.

When the helicity amplitudes are decomposed into partial waves,[10]

$$\mathrm{Im}\phi_1(0) = \frac{1}{k} \sum_J \mathrm{Im}\{(2J + 1)R_J + (J + 1)R_{J+1,J} + JR_{J-1,J} + 2[J(J+1)]^{1/2}R^J\}, \quad (4)$$

$$\mathrm{Im}\phi_2(0) = \frac{1}{k} \sum_J \mathrm{Im}\{-(2J + 1)R_J + (J + 1)R_{J+1,J} + JR_{J-1,J} + 2[J(J+1)]^{1/2}R^J\}, \quad (5)$$

and

$$\mathrm{Im}\phi_3(0) = \frac{1}{k}\sum_J \mathrm{Im}\{(2J+1)R_{JJ} + JR_{J+1,J} + (J+1)R_{J-1,J} - 2[J(J+L)]^{1/2}R^J\}, \quad (6)$$

where R_J is the spin-singlet partial-wave amplitudes with $J = L =$ even, R_{JJ} and $R_{J\pm 1,J}$ are spin-triplet waves with $J = L =$ odd and $J = L \mp 1 =$ even, respectively, and R^J is the mixing term. The partial wave characteristics to $\phi_1(0)$ is R_J and to $\phi_3(0)$ is R_{JJ}; the peak in Fig. 3a is due to one of the singlets $^1S_0$, $^1D_2$,..., and the dip is due to one of the triplets $^3P_1$, $^3F_3$,... .

III. Structure in σ_{el}^{Tot} and Polarization

So far, such a behavior is discussed only at $|t| = 0$, and the properties of the possible resonance (e.g., spin and parity) are not determined. One needs to study the angular distributions of the observables in pp scattering. Let us see if we observe a similar structure in other channels. Figure 7 shows the elastic total cross section, σ_{el}^{Tot}.[11,12] There is also a structure in the

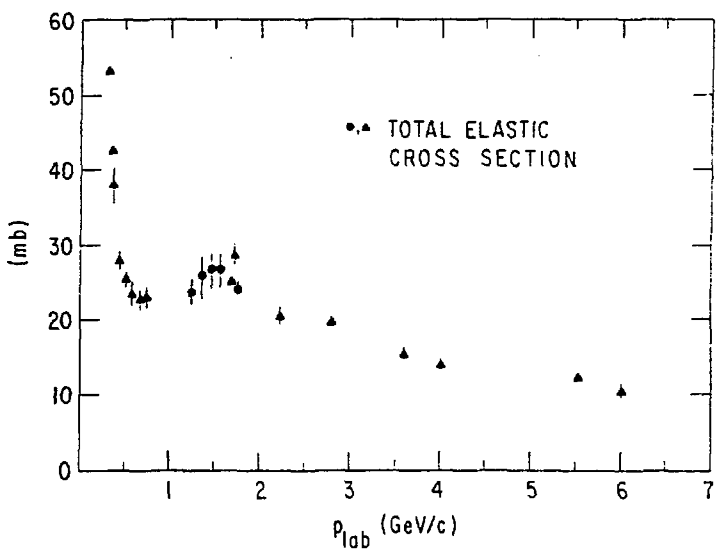

Fig. 7 Elastic total cross section.

plot of polarization against incident momentum at fixed $|t|$, as shown in Fig. 8.[13] We note that the structure in polarization has nothing to do with the peak in $\Delta\sigma_L$ at 1.2 GeV/c, because the polarization does not include singlet terms.

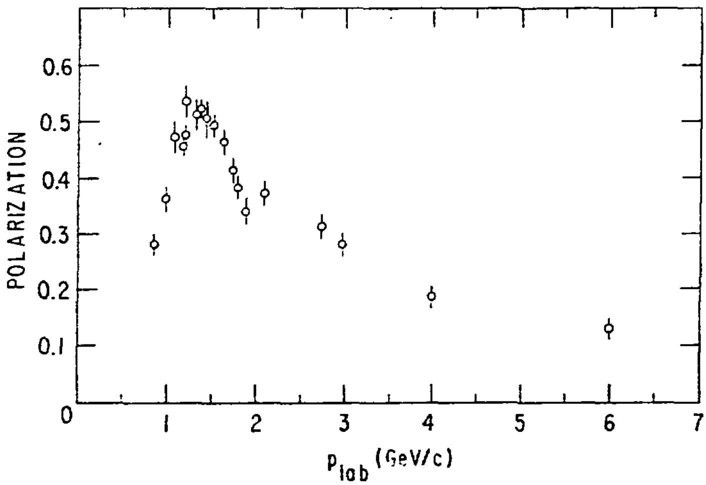

Fig. 8 Polarization at $0.1 < |t| < 0.2$.

IV. Legendre Coefficient Analysis

Using polarization data, we investigate whether an R_{JJ} partial wave has the behavior of the Breit-Wigner formula.[10] The effect of resonance can be studied through the energy dependence of the Legendre expansion coefficients obtained from the product of differential cross-section and polarization data.[12,13] We expand differential cross sections and polarization as follows:

$$d\sigma/d\Omega = 1/k^2 \sum_{n=0}^{\infty} a_n P_n (\cos\theta) \text{ and} \tag{7}$$

$$P\, d\sigma/d\Omega = 1/k^2 \sum_{n=2}^{\infty} b_n P_n^{(1)} (\cos\theta) \quad . \tag{8}$$

Note that, because of symmetries, n must be even. All the observed coefficients a_n and b_n with $n \geqq 8$ almost vanish in p_{lab} = 1.0 - 2.0 GeV/c. This means we can ignore partial waves with $J > 4$ and $L > 4$ in this energy range. Therefore the possible R_{JJ} resonance is $R_{11} = {}^3P_1$ or $R_{33} = {}^3F_3$. As shown in Fig. 9, all the coefficients b_n have a strong energy dependence around 1.5 GeV/c, where $\Delta\sigma_L$ has the prominent structure. We examine whether ${}^3P_1$ or ${}^3F_3$ resonance can explain all these structures by studying each coefficient. The coefficients a_n and b_n are expressed in terms of partial-wave amplitudes (see Ref. 14).

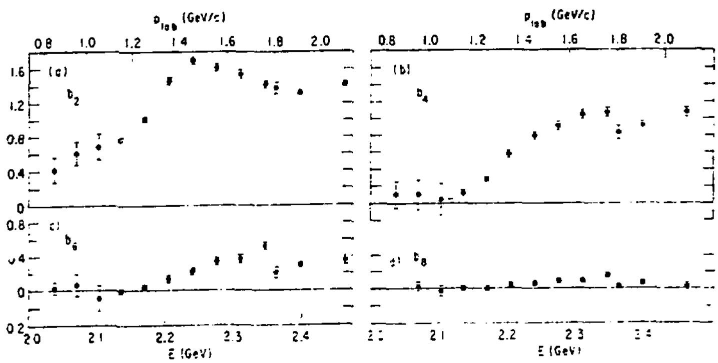

Fig. 9 Results of Legendre coefficient analysis of polarization data; the coefficient b_n of Eq. 8 vs. laboratory momentum.

Coefficient b_6

The coefficient b_6 is related with partial-wave amplitudes as follows:

$$b_6 = 1.8\ (\mathrm{Im}\,^3F_3 \mathrm{Re}\,^3F_4 - \mathrm{Re}\,^3F_3 \mathrm{Im}\,^3F_4) + \ldots\ , \tag{9}$$

where the residual terms (...) include neither $^3F_3$ nor $^3P_1$. A rapid increase with energy in b_6 can be explained with the $^3F_3$ wave following the Breit-Wigner formula and the other amplitudes varying slowly with energy. By unitarity, $\mathrm{Im}\,^3F_4$ is positive. Therefore, if we assume that the $^3F_3$ wave has a Breit-Wigner behavior such as

$$^3F_3 = \frac{\varepsilon + 1}{\varepsilon^2 + 1}\ \frac{\Gamma_{e\ell}}{\Gamma} \tag{10}$$

with $\varepsilon = 2(M - E)/\Gamma$, M = 2260 MeV, and Γ = 200 MeV, then each term of Eq. 9 behaves as shown in Fig. 10. In any case, the sum of the first two terms increases rapidly with energy a whole. Here note that $^3P_1$ resonance can not explain this increase with energy because b_6 does not include the $^3P_1$ wave.

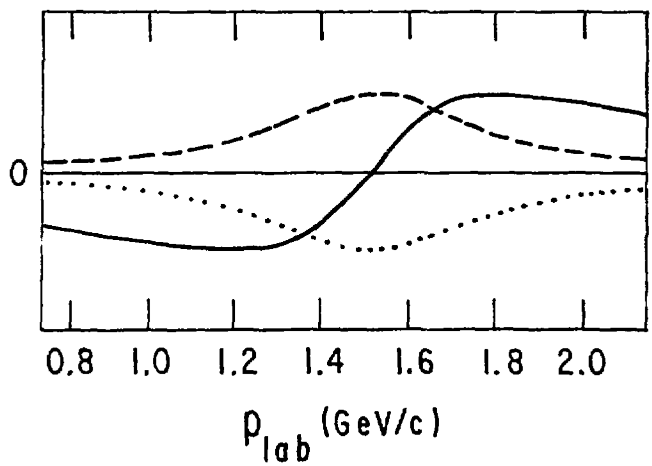

Fig. 10 Plots of each term of Eq. 9 against laboratory momentum (vertical scale is arbitrary). Solid curve represents the second term -1.8 $(\mathrm{Re}\,^3F_3)(\mathrm{Im}\,^3F_4)$. Dashed curve and dotted curve show the first term $1.8(\mathrm{Im}\,^3F_3)(\mathrm{Re}\,^3F_4)$ corresponding to positive and negative $\mathrm{Re}\,^3F_4$ respectively.

Coefficients b_2 and b_4

Here we examine whether the structure in b_2 and b_4 can be interpreted with $^3F_3$ following the Breit-Wigner formula of Eq. 10. In terms of partial-wave amplitudes, b_2 and b_4 are given as:

$$b_2 = (\mathrm{Im}\,{}^3F_3)(\mathrm{Re}A) - (\mathrm{Re}\,{}^3F_3)(\mathrm{Im}\,A) + (\text{terms without } {}^3F_3) \tag{11}$$

and

$$b_4 = (\mathrm{Im}\,{}^3F_3)(\mathrm{Re}A') - (\mathrm{Re}\,{}^3F_3)(\mathrm{Im}\,A') + (\text{terms without } {}^3F_3) \,, \tag{12}$$

where

$$A = 2.0\ {}^3P_2 - 2.0\ {}^3F_2 + 0.8\ R^2 + 2.8\ {}^3F_4 \tag{13}$$

$$A' = 1.2\ {}^3P_2 - 1.5\ {}^3F_2 + 0.6\ R^2 + 2.5\ {}^3F_4 \tag{14}$$

In the region around 1.5 GeV/c, both phase-shift analyses of MacGregor et al.[15] and Hoshizaki[16,17] give

$$\mathrm{Re}\,A \gg \mathrm{Im}\,A > 0 \tag{15}$$

$$\mathrm{Re}\,A' \gg \mathrm{Im}\,A' > 0 \ . \tag{16}$$

The second term in Eqs. 11 and 12 can be neglected, and the first term in the same equations has a peak at 1.5 GeV/c. We therefore expect b_2 and b_4 to have a bump around 1.5 GeV/c. Indeed, b_2 and b_4 have such a behavior, as shown in Fig. 9. Thus we can say that strong energy dependences of b_2, b_4 and b_6 can be explained with $^3F_3$ consistent with the Breit-Wigner formula. From $\Delta\sigma_L$ data we can estimate the elasticity $\Gamma_{e\ell}/\Gamma$ of the possible $^3F_3$ resonances as 0.15-0.25.

V. $C_{LL} = (L,L;0,0)$ Measurements

Simultaneously with $\Delta\sigma_L$ measurements, we have measured the spin-spin correlation parameter $C_{LL}(\theta_{c.m.}) = (L,L;0,0)$ in p-p elastic scattering for $70° \leq \theta_{c.m.} \leq 110°$ at $p_{lab} = 1.0$ to 3.0 GeV/c.[18] A typical experimental setup is shown in Fig. 2(b).

The differential cross section for a particular spin direction of beam and target, $I^{\pm\pm}$, is given by

$$I^{\pm\pm}(\theta_{c.m.}) = I_0(\theta_{c.m.}) \, [1 + (\pm P_B)(\pm P_T) C_{LL}(\theta_{c.m.})] \, , \tag{17}$$

where P_B and P_T are the beam and target polarization respectively, and + (-) refers to the spin state parallel (antiparallel) to the L direction (beam direction); $I_0(\theta_{c.m.})$ is the spin-averaged differential cross section. The parameter $C_{LL}(\theta_{c.m.})$ is then found to be

$$C_{LL}(\theta_{c.m.}) = \frac{1}{P_B P_T} \; \frac{(I^{++} + I^{--}) - (I^{+-} + I^{-+})}{(I^{++} + I^{--}) + (I^{+-} + I^{-+})} \; . \tag{18}$$

The values of the parameter C_{LL} at various incident-beam momenta are all positive over the angular range covered, and are consistent with a symmetry about $\theta_{c.m.} = 90°$ as expected for scattering of identical particles.

The values of C_{LL} at $\theta_{c.m.} = 90°$ are plotted with respect to the incident momenta as shown in Fig. 11. We observe a sharp dip near p_{lab} = 1.2 GeV/c, rapid decrease near 1.5 GeV/c, and additional structure near p_{lab} = 2.0 GeV/c. A way to study these structures is to define C_{LL} in terms of partial wave amplitudes. Using the s-channel helicity amplitudes $\phi_1 = \langle ++|\phi|++\rangle$, $\phi_2 = \langle --|\phi|++\rangle$, $\phi_3 = \langle +-|\phi|+-\rangle$, $\phi_4 = \langle +-|\phi|-+\rangle$, and $\phi_5 = \langle ++|\phi|+-\rangle$, we have

$$C_{LL}(d\sigma/d\Omega) = 1/2[-|\phi_1|^2 - |\phi_2|^2 + |\phi_3|^2 + |\phi_4|^2] \quad , \tag{19}$$

where $d\sigma/d\Omega = 1/2[|\phi_1|^2 + |\phi_2|^2 + |\phi_3|^2 + |\phi_4|^2 + 4|\phi_5|^2]$ is the spin-averaged differential cross section.

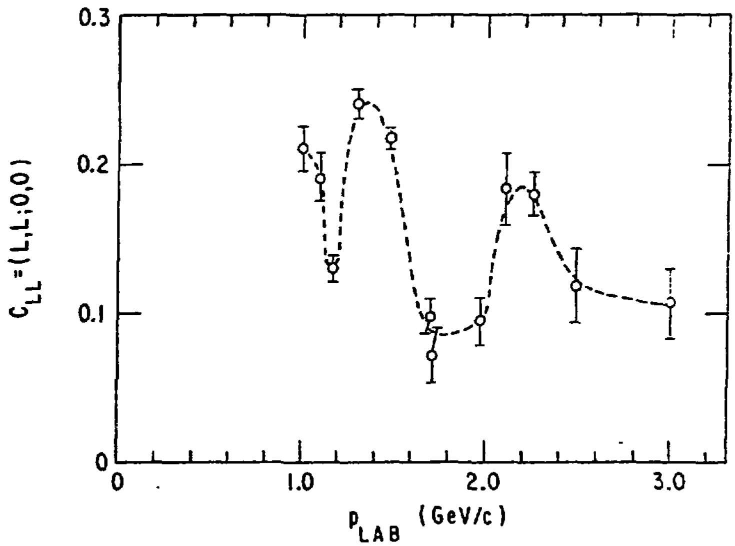

Fig. 11 C_{LL} = (L,L;0,0) at $\theta_{c.m.}$ = 90°

The amplitudes ϕ_1 through ϕ_5 are then expanded in terms of partial wave amplitudes. The spin-singlet partial waves, $^1S_0$, $^1D_2$, $^1G_4$ ..., appear in ϕ_1 and ϕ_2 with opposite signs, and the spin-triplet partial waves with $L = J =$ odd, $^3P_1$, $^3F_3$, ..., appear in ϕ_3 and ϕ_4 with opposite signs.

Figure 12a shows the quantity on $k^2C_{LL}(d\sigma/d\Omega)$ at $\theta_{c.m.}$ = 90° plotted with respect to the incident momenta.[19] This quality is dimensionless and allows us to study the contributions of partial waves more directly.

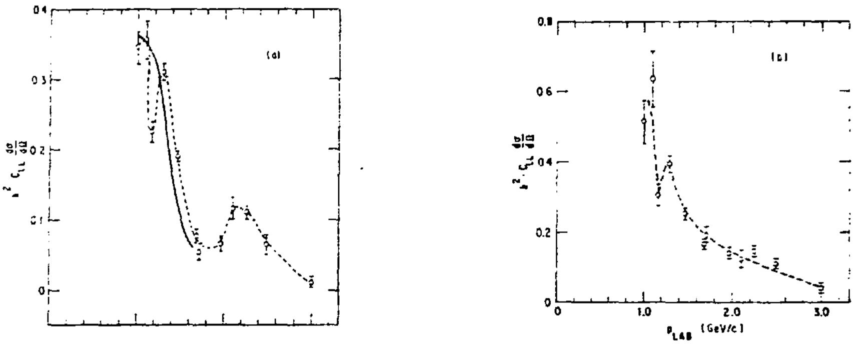

Fig. 12 (a) $k^2 C_{LL}$ $(d\sigma/d\Omega)$ at $\theta_{c.m.} \approx$ vs. p_{lab}. The dashed curve is only to guide the eye. The solid curve is the contribution of the $^3F_3$ resonance over a smooth background.

(b) $k^2 C_{LL}$ $(d\sigma/d\Omega)$ at $\theta_{c.m.} \approx 74°$ vs. p_{lab}. The dashed curve is only to guide the eye.

First we examine if the rapid decrease in Figs. 11 and 12a near p_{lab} = 1.5 GeV/c is consistent with the partial wave $^3F_3$ having a resonant behavior.[10] Eq. 19 can be expressed in terms of $^3F_3$ and interfering partial waves as

$$[k^2 C_{LL}(d\sigma/d\Omega)]_{90°} = [0.77|^3F_3|^2 + a(\mathrm{Re}\,^3F_3) + b(\mathrm{Im}\,^3F_3) + \ldots], \qquad (20)$$

where (b) is the real (imaginary) part of the sum of other partial waves and the values can be estimated from the results of a phase-shift analysis.[17,20] By substituting these values and the $^3F_3$ resonance at mass = 2260 MeV with a width = 200 MeV and elasticity = 0.2 into Eq. 20, we find the same amount of rapid decrease as shown in Fig. 12a.

Next, we discuss the structure around p_{lab} = 2 GeV/c in Fig. 12a. From the resonant-like structure in $(k^2/4\pi)\Delta\sigma_T$ as shown in Fig. 5, we expect it is due to a singlet spin state.[7,8] The contribution of spin singlet waves to Eq. 19 is

$$k^2 C_{LL}(d\sigma/d\Omega) = -|{}^1S_0 + 5\ {}^1D_2 P_2(\cos\theta) + 9\,{}^1G_4 P_4(\cos\theta) + \ldots|^2 + \ldots\ , \quad (21)$$

in which the contribution of ${}^1G_4$ vanished at $\theta \gtrsim 70°$, where $P_4 = 0$.

The structure around 2 GeV/c is absent in Fig. 12(b), where the values of $k^2 C_{LL}$ $d\sigma/d\Omega$ at $\theta_{c.m.} = 70°$ are plotted as a function of beam momentum. Thus we may conclude that ${}^1G_4$ wave is responsible for the structure.

Next, we discuss the sharp dip observed at 1.17 GeV/c as shown in Figs. 12a and 12b. We consider this due to a spin-singlet wave, because structures also appear as a peak both in $\Delta\sigma_L$ and $\Delta\sigma_T$.[7,8] In particular, we suspect they are due to the ${}^1D_2$ wave, because it is the only wave that couples to the s wave NΔ state, which is responsible for the rapid increase of pp total cross section near 1.2 GeV/c. We also point out that a resonance-like bump was observed in the cross-section of $pp \to \pi d$ in the same energy range,[21] which is usually interpreted in terms of the final-state interaction between one of the nucleons and π, forming $\Delta(1236)$ in the intermediate state.

The dip structure in Figs. 12a and 12b may come from the resonant-like behavior of the ${}^1D_2$ state.[16,17,20,22]

We conclude that the measurement of the spin-spin correlation parameter C_{LL} in pp elastic scattering near $\theta_{c.m.} = 90°$ has revealed rich structure in $p_{lab} = 1.0 - 3.0$ GeV/c, which is consistent with the presence of ${}^3F_3$, and possibly ${}^1G_4$ and ${}^1D_2$ resonances.

VI. C_{NN} = (N,N;0,0) Measurements at $\theta_{c.m.}$ = 90°

The measurement of the spin-spin correlation parameter C_{NN} in pp elastic scattering at $\theta_{c.m.}$ = 90° also reveals a strong energy dependence. A plot of k^2C_{NN} $(d\sigma/d\Omega)$ in the momentum region 1 to 6 GeV/c is shown in Fig. 13.[23,24] We find that the energy dependence is consistent with the existence of $^1D_2$ and $^3F_3$ resonances.

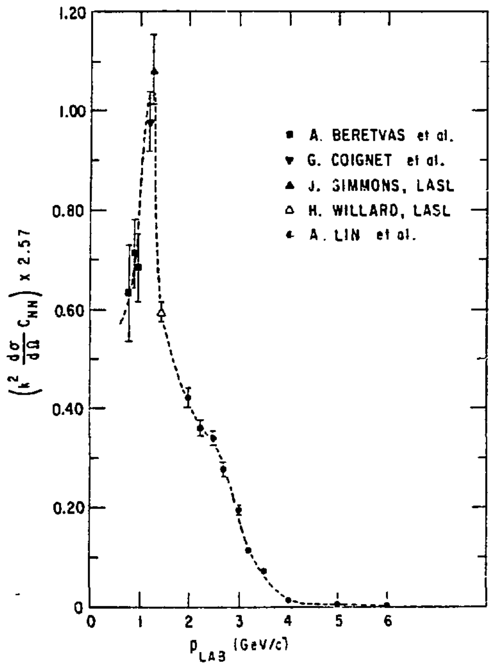

Fig. 13 k^2C_{NN} $(d\sigma/d\Omega)$ at $\theta_{c.m.}$ = 90°.

VII. Real Part of Scattering Amplitude at $|t|$ = 0

The real part of scattering amplitude in the forward region in pp elastic scattering has been experimentally determined.[25] A plot of Re/Im at $|t| = 0$ is shown in Fig. 14. The real part changes from positive to negative as energy increases and becomes zero at around 1.5 GeV/c. The behavior is consistent with the existence of $^1D_2$ and $^3F_3$ resonances.[17]

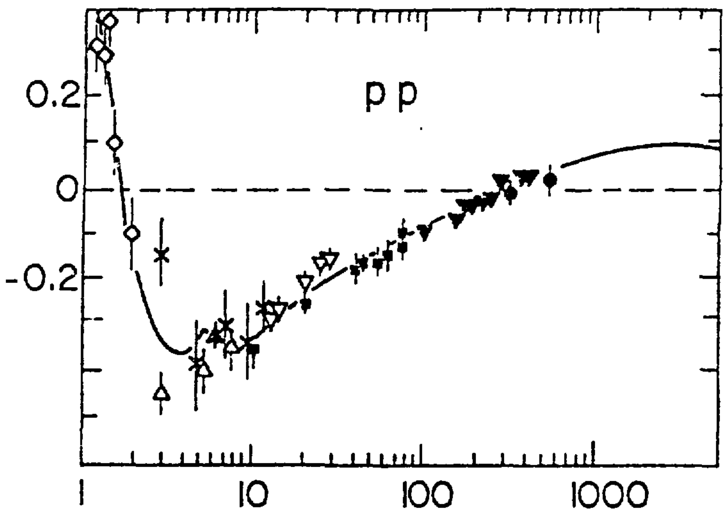

Fig. 14 Re/Im at $|t| = 0$.

VIII. pp Phase-Shift Analyses

During the past several years, there has been a concentrated effort in pp phase-shift analyses. Hoshizaki established evidence for the existence of resonances in his phase-shift analysis.[17] Indication of diproton resonances in the $^3F_3$ (2.22 GeV) and $^1D_2$ (2.17 GeV) states is shown in Fig. 15. Arndt[20] recently extended and revised his phase-shift analysis up to 750 MeV for the energy-independent analysis and to 850 MeV for the energy-dependent analysis. His results give strong indication of resonances in the $^1D_2$ and $^3F_3$ states as shown in Fig. 16.

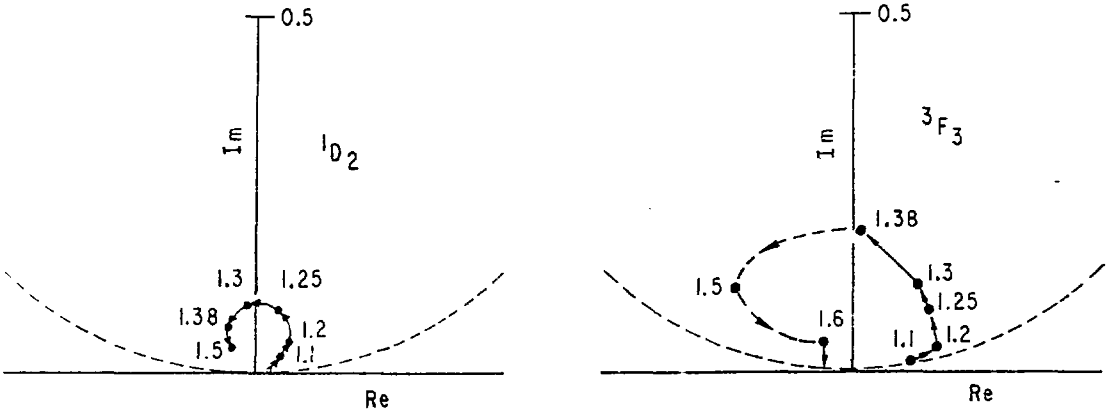

Fig. 15 Argand diagrams of the $^1D_2$ and $^3F_3$ partial waves; the background contributions have been subtracted.[17]

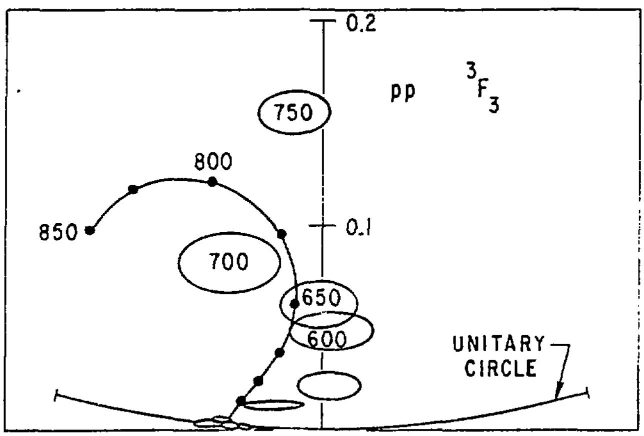

(Figure caption on following page)

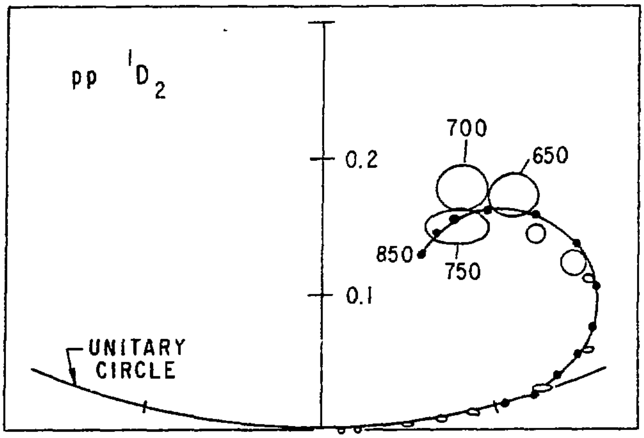

Fig. 16 Argand diagrams of the $^3F_3$ and $^1D_2$ partial waves based on Arndt's phase shifts. The elipses represent the errors in the real and imaginary parts of the amplitudes for energy-independent solutions. The continuous curves represent the energy-dependent solutions.

Since then, additional evidence for the existence of dinucleons has become available. These new findings are covered below.

IX. Other Structure in the pp System (I = 1)

As discussed earlier, $\Delta\sigma_T$ data contain only singlet structures. Then we expect to see only the triplet structure in $(\Delta\sigma_T - \Delta\sigma_L)$, as shown in Fig. 17. We observe a new triplet structure at 2.0 GeV.c in addition to the one at 1.5 GeV/c (see Fig. 18). We can deduce that the quantum number of the triplet peak at 2.0 GeV/c is as follows: The absence of this structure in $\Delta\sigma_L$ suggests that, from Eqs. 4 and 6, either i) $(2J + 1)R_J = (2J + 1)R_{JJ}$ or ii) $(2J + 1)R_J = R_{J-1,J}$. We can eliminate the latter possibility by examining Eq. 5 from the fact that there is a peak in $\Delta\sigma_T$ at 2 GeV/c. Therefore the triplet peak at 2.0 GeV/c is due to a partial wave R_{JJ}.

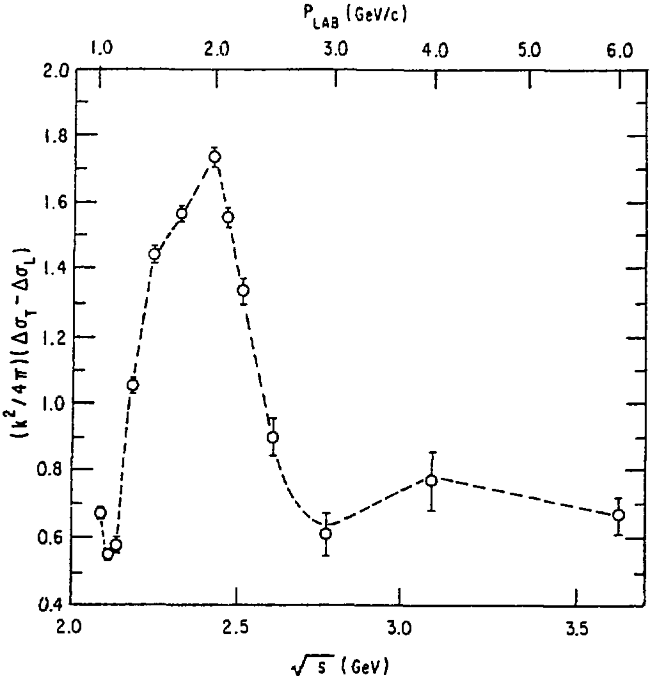

Fig. 17 $(k^2/4\pi)(\Delta\sigma_T - \Delta\sigma_L)$

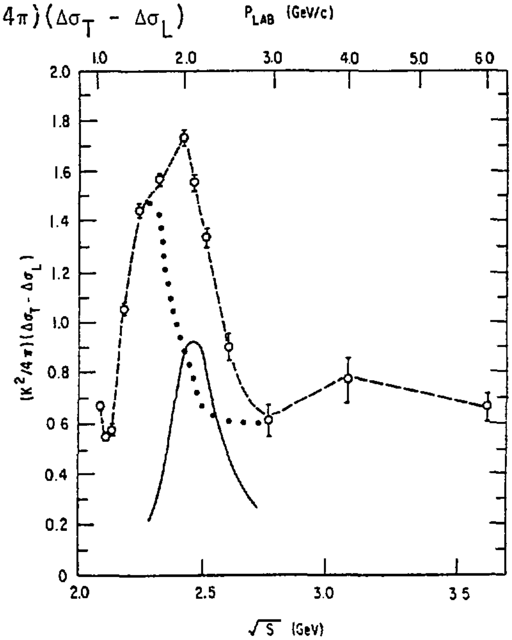

Fig. 18 New triplet structure at 2.0 GeV/c; the dotted curve is deduced from $\Delta\sigma_L$ data.

We note that there is no $^3F_3$ partial-wave contribution to the polarization data at $\theta_{c.m.} = 63°$. We see an interesting structure in a plot of $k^2P\ (d\sigma/d\Omega)/\sin 2\theta_{c.m.}$ vs. p_{lab} as shown in Fig. 19. This quantity is proportional to

$$(2\ \mathrm{Im}\ ^3P_0 + 3\ \mathrm{Im}\ ^3P_1)(\mathrm{Re}\ ^3P_2) - (2\ \mathrm{Re}\ ^3P_0 + 3\ \mathrm{Re}\ ^3P_1)(\mathrm{Im}\ ^3P_2)\ .$$

Since the $^3P_2$ partial wave has very little energy dependence, there is a good chance that either $^3P_0$ or $^3P_1$ might be resonating.

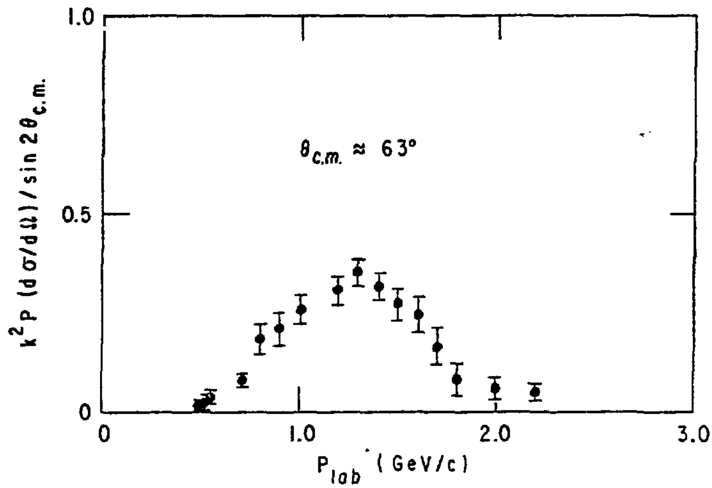

Fig. 19 Energy dependence of $P(d\sigma/d\Omega)$ at $\theta_{c.m.} \gtrsim 63°$

Do we observe any structure above a mass of 2500 MeV? Measurements of $\Delta\sigma_L$ and $\Delta\sigma_T$ are yet to be made at small-momentum interval. However, we observe a remarkable energy dependence in $C_{NN} = (N,N;0,0)$ data at all angles[26] and also at $\theta_{c.m.} = 90°$.[24] As shown in Fig. 11, C_{LL} data are all positive at large angles up to 3.0 GeV/c, but we observe negative values as large as -35% at 6 GeV/c.[27]

X. $\Delta\sigma_L$(I=0) Measurements

An Argonne group[28] has recently measured the difference between isoscaler nucleon-nucleon total cross sections for pure longitudinal initial spin states, $\Delta\sigma_L(I = 0)$, using a polarized proton beam and a polarized deuteron target. In the $\Delta\sigma_L(I = 0)$ preliminary data, as shown in Fig. 20, a significant structure is observed around 1.5 GeV/c. This seems to suggest the existence of a new isoscalar spin-singlet dinucleon resonance. We note here that there exists a clear bump in the np total cross-section data[29] in the vicinity of 1.5 GeV/c as shown in Fig. 21.

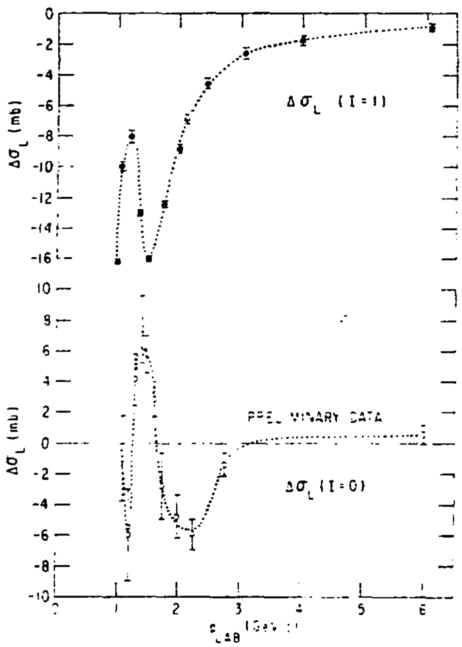

Fig. 20 $\Delta\sigma_L(I = 0)$ together with $\Delta\sigma_L(I = 1)$.

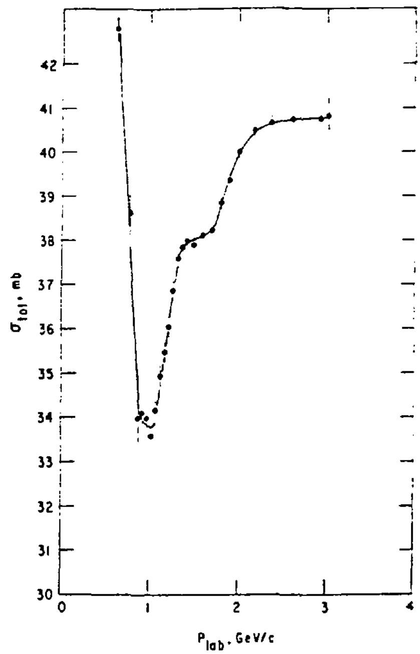

Fig. 21 np total cross section.

A recent phase-shift analysis using these preliminary data by Hoshizaki et al.[30] suggests that there exists a partial wave whose behavior is consistent with the Breit-Wigner resonance formula, namely, the spin-singlet $^1F_3$ wave. From the dispersion analysis of a forward I = 0 scattering amplitude using the data on $\Delta\sigma_L(I = 0)$, Grein and Kroll showed that the Argand plot of the amplitude has a resonancelike behavior around 1.5 GeV/c, and that suggests the existence of a spin-singlet dibaryon resonance.

XI. Conclusion on I = 0 and I = 1 Resonances

Dibaryon resonances that can couple to nucleon-nucleon systems are summarized below. The name, B^2, of resonances was adopted during the 1978 International Tokyo conference.

i) I = 1

	B_1^2 (2.14)	B_1^2 (2.18)	B_1^2 (2.22)	B_1^2 (2.43)	B_1^2 (2.43)
Mass, GeV	2.14 - 2.17	2.18 - 2.20	2.20 - 2.25	2.43 - 2.50	2.43 - 2.50
Width, MeV	50 - 100	100 - 200	100 - 200	~150	~150
I = 1 State	$^1D_2$	Triplet P	$^3F_3$	$^1G_4$	R_{JJ}

ii) I = 0

	B_0^2 (2.14)	B_0^2 (2.22)	B_0^2 (2.43)
Mass, GeV	2.14 - 2.17	2.20 - 2.26	2.40 - 2.50
Width, MeV	50 - 100	100 - 200	
I = 0 State	Triplet	$^1F_3$	Triplet

In order to clarify the nature of I = 1 B^2 (2.18), B^2 (2.43) singlet, and B^2 (2.43) triplet, a number of measurements on C_{LL}, C_{SL} etc. covering all angles have been carried out from 1- to 2.5-GeV/c incident momenta. These data should be available within a year.

XII. Possible Dibaryon Resonance in γd Scattering Experiment

Kamae et al.[31] suggested the possible existence of a dinucleon resonance by measuring the proton polarization in the reaction $\gamma d \rightarrow p_{\uparrow} n$. They observed an energy dependence in the polarization. They interpret some of the data as an indication of an existence of a deeply bound Δ-Δ state. Their estimates of mass and width of the possible resonance are 2380 and 200 MeV. From the angular dependence of their polarization data, they estimated spin parity and isospin as $(J^P, I) = (3^+, 0)$. They obtained reasonable fits to the polarization data by introducing their dibaryon resonance with mass around 2380 MeV in addition to the $^3F_3$ dinucleon resonance with mass around 2260 MeV described in previous pages. Without the $^3F_3$ resonance, they could not obtain good fits by using only one resonance of 2380 MeV. This fact also supports the $^3F_3$ diproton-resonance picture.

XIII. Other References on Dibaryons

Other authors have suggested the possibility of the existence of diproton resonances. R. Kammerud et al. analyzed the data of large-angle proton-proton elastic scattering at intermediate momenta, and they speculated the existence of dibaryon masses at about 2.2, 2.6, 3.4 and 3.9 GeV by observing slope changes in $d\sigma/dt$.[32] A similar conclusion was also drawn earlier by L. M. Libby and E. Predazzi.[33] K. Kanai et al. show that there are effects of dinucleon resonances in πd elastic scattering.[34] The effects are clearly seen in the angular region of $\theta_{c.m.} > 100°$. H. Kamo and W. Watari find effects of dinucleon resonances in the polarization data in $pp \rightarrow \pi d$ reaction.[35] R. Frascaria et al. observe dinucleon-resonance signals in the $\pi^+ d$ excitation function of 180°.[36] T. Ueda et al. discuss the existence of dinucleon resonances in πNN and $\pi\pi NN$ dynamics.[37] S. Furuichi et al. investigated channel coupling effects in relation to the exotic resonances.[38]

XIV. Are There Lower-Mass Narrow-Width Dibaryon Resonances Than Those Described Above?

At CERN there will be a LEAR (low energy $\bar{p}$ ring) facility which will allow total cross-section measurements in the $\bar{p}p$ system at small steps in the momentum range of 0.1-2 GeV/c.

How well were the total cross-section measurements in the pp system done? As shown in Fig. 22, pp total cross sections were not well measured. A narrow-width structure could have been overlooked. For instance, the energy region of 2020- and 2060-MeV resonances, which are on MacGregor's diproton trajectory,[40] was not well covered. We illustrate a possible resonance with width $\gtrsim$ 15 MeV in Fig. 22. It seems highly desirable to make precision pp total cross-section measurements with small energy intervals.[41]

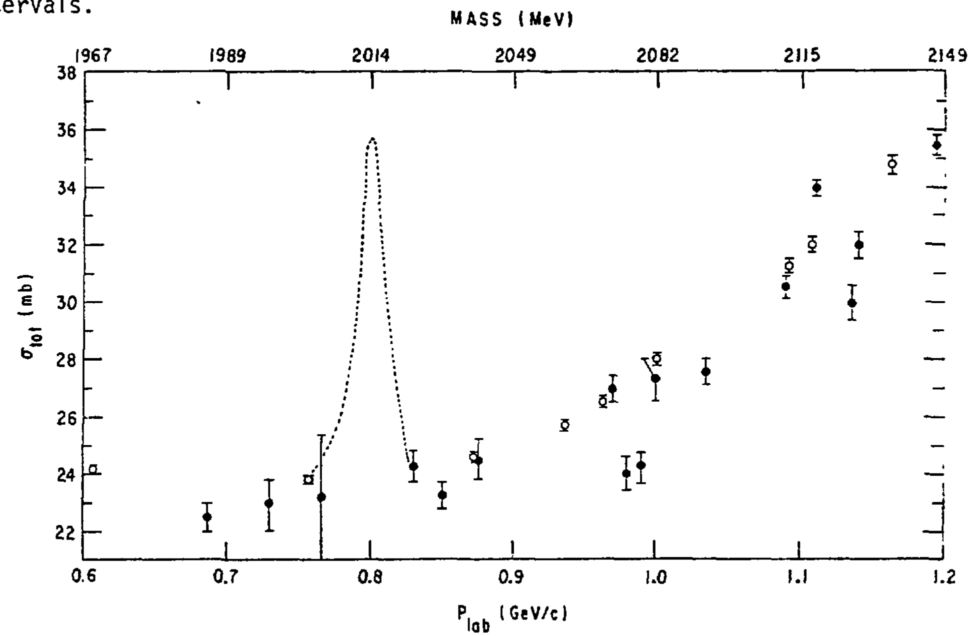

Fig. 22 pp total cross section at intermediate energies (black circles: G. Giacomelli; white circles: P. Schwaller et al.).[39]

XV. Quark-Models and Dibaryons

Several models predict the existence of dinucleon resonances. For example, i) the bag model predicts a dibaryon resonance, which is made of six quarks inside a cavity, depicted in Fig. 23; e.g. Aerts et al.[2] predicted many dinucleon resonances with mass of 2.1 to 2.5 GeV.

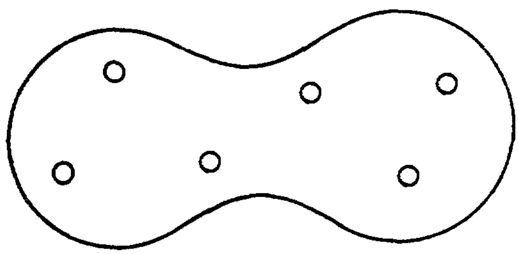

Fig. 23 Dibaryon resonance in bag model. Solid line and circles represent cavity and quarks respectively.

ii) The string model[42] gives a dibaryon resonance, which is made of six quarks combined together with strings, such as shown in Fig. 24.

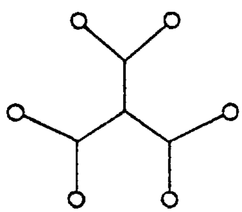

Fig. 24 Dibaryon resonance in string model.

Dinucleon resonances open a new era in the nucleon-nucleon system and are also crucially important for further development of the quark models.

REFERENCES

1. R. L. Jaffee, Phys. Rev. Lett. 38, 195 (1977) and Errata 38, 617 (1977).

2. P. J. G. Mulders, A. Th. M. Aerts, and J. J. DeSwart, Phys. Rev. Lett. 40, 1543 (1978).

3. H. Lipkin, private communication; F. Myhrer, to be published.

4. D. B. Lichtenberg et al., Phys. Rev. D18, 2569 (1978); S. Ishida and M. Oda, Prog. Theor. Phys. 61, 1401 (1979).

5. I. P. Auer et al., Phys. Lett. 67B, 113 (1977).

6. I. P. Auer et al., Phys. Lett. 70B, 475 (1977).

7. I. P. Auer et al., Phys. Rev. Lett. 41, 354 (1978).

8. For $\Delta\sigma_T$ data see W. deBoer et al., Phys. Rev. Lett. 34, 558 (1975); E. K. Biegert et al., Phys. Lett. 73B, 235 (1978).

9. W. Grein and P. Kroll, Nucl. Phys. B137, 173 (1978); P. Kroll, University of Wuppertal preprint WUB 78-13 (1978).

10. K. Hidaka et al., Phys. Lett. 70B, 479 (1977).

11. A compilation of NN and ND interactions, UCRL-20000 NN (1970).

12. To obtain the total elastic cross section from 1.2 to 1.7 GeV/c, we have integrated the differential cross-section data by B. A. Ryan et al., Phys. Rev. 3, 1 (1971). These data were used because of internal consistency.

13. M. G. Albrow et al., Nucl. Phys. B23, 445 (1970).

14. K. Hidaka and A. Yokosawa, Surveys in High Energy Physics, London, England (1979).

15. M. H. MacGregor et al., Phys. Rev. 169, 1149 (1968).

16. N. Hoshizaki, Prog. Theor. Phys. 57, 1099 (1977); 58, 716 (1977).

17. N. Hoshizaki, Prog. Theor. Phys. 60, 1796 (1978); 61, 129 (1979).

18. I. P. Auer et al., Phys. Rev. Lett. 41, 1436 (1978).

19. Differential cross section data: B. A. Ryan et al., Phys. Rev. D3, 1 (1971); D. T. Williams et al., Nuovo Cimento, 8A, 447 (1972); K. Abe et al., Phys. Rev. 12D, 1 (1975); M. G. Albrow et al., Nucl. Phys. B23, 445 (1970).

20. R. A. Arndt, Talk given during LAMPF Nucleon-Nucleon Workshop, July, 1978; also private communication (1979).

21. M. G. Mescheryakov, B. S. Neganov, N. P. Bogachev, and V. M. Sidorov, Dokl, Akad. Nauk SSSR 100, 673 (1955); M. G. Mescheryakov and B. S. Neganov, Kokl. Akad. Nauk SSSR 100, 677 (1955); B. S. Neganov and L. B. Parfernov, Zh. Esperrim, i Teor Fiz. 34, 767 (1958) (translation: Soviet Phys. - JETP 7, 528 (1958).

22. R. A. Arndt, Phys. Rev. 165, 1834 (1968); G. L. Kane and G. H. Thomas Phys. Rev. D 13, 2944 (1976); L. M. Libby and E. Predazzi,Lettere Al Nuovo Cimento, Vol. II, N. 18, 881 (1969); J. H. Hall et al., Nucl. Phys. B12, 573 (1969); H. Suzuki, Prog. Theor. Phys. 54, 143 (1975) and earlier references therein.

23. A. Beretvas et al., Rev. Mod. Phys. 39, 536 (1967); G. Coignet et al.; J. Simmons et al; H. Willard et al.

24. A. Lin et al., Phys. Lett. 74B, 273 (1978).

25. U. Amaldi, M. Jacob and G. Matthiae, Ann. Rev. Nucl. Sci. 26, 385 (1976).

26. D. Miller et al., Phys. Rev. Lett. 36, 763 (1976); Phys. Rev. D 16, 2016 (1977).

27. I. P. Auer et al. to be published.

28. D. Underwood et al., Bull. of Am. Phys. Soc. 24, 636 (1979); also to be published.

29. T. J. Devline et al., Phys. Rev. D 8, 136 (1973).

30. N. Hoshizaki et al., in these proceedings.

31. T. Kamae et al., Phys. Rev. Lett. 38, 471 (1977); H. Ikeda et al., Phys. Rev. Lett. 42, 1321 (1979); K. Nakamura, in these proceedings.

32. R. C. Kammerud et al., Phys. Rev. D 4, 1309 (1971).

33. L. M. Libby and E. Predazzi, Lett. Al Nuovo Cimento, Vol. II, 831 (1969).

34. K. Kanai et al., Prog. Theor. Phys. 62, 153 (1979); also see K. Kubodera et al., Phys. Lett. 87B, 169 (1979).

35. H. Kamo and W. Watari, Prog. Theor. Phys. 62, 843 (1979).

36. R. Frascaria et al., to be published.

37. T. Ueda, Phys. Lett. 74B, 123 (1978); Phys. Lett. 79B, 487 (1978); M. Araki et al., Prog. Theor. Phys. 63, No. 1 (1980).

38. S. Furuichi et al., Proceedings of the Meeting on Exotic Resonances, Hiroshima, Japan (1978), HUPD-7813.

39. G. Giacomelli, Prog. in Nucl. Phys., 12, 214 (1971); P. Schwaller et al., Nucl. Phys. A316, 317 (1979).

40. M. H. MacGregor, Phys. Rev. Lett. 42, 1724 (1979).

41. T. H. Fields and A. Yokosawa, to be published in Phys. Rev. (1980).

42. M. Imachi et al., Prog. Theor. Phys. 55, 551 (1976); 57, 517 (1977); S. Ishida and M. Oda, Prog. Theor. Phys. 60, 828 (1978); 61, 1401 (1979).